HHS Public Access

Author manuscript

Clin Cancer Res. Author manuscript; available in PMC 2022 October 04.

Published in final edited form as:

Clin Cancer Res. 2021 March 01; 27(5): 1399–1409. doi:10.1158/1078-0432.CCR-20-3453.

^{177}Lu-DOTA-EB-TATE, A Radiolabeled Analog of Somatostatin Receptor Type 2, for the Imaging and Treatment of Thyroid Cancer

Shilpa Thakur[1], **Brianna Daley**[1], **Corina Millo**[2], **Craig Cochran**[1], **Orit Jacobson**[3], **Huiyan Lu**[4], **Zhantong Wang**[5], **Dale O. Kiesewetter**[3], **Xiaoyuan Chen**[5], **Vasyl Vasko**[6], **Joanna Klubo-Gwiezdzinska**[1,*]

[1]Metabolic Disease Branch, National Institute of Diabetes and Digestive and Kidney Diseases, National Institutes of Health, Bethesda, MD, USA.

[2]Clinical Center, National Institutes of Health, Bethesda, MD, USA.

[3]Molecular Tracer and Imaging Core Facility, National Institute of Biomedical Imaging and Bioengineering, National Institutes of Health, Bethesda, MD, USA.

[4]National Institute of Diabetes and Digestive and Kidney Diseases, National Institutes of Health, Bethesda, MD, USA.

[5]Laboratory of Molecular Imaging and Nanomedicine, National Institute of Biomedical Imaging and Bioengineering, National Institutes of Health, Bethesda, MD, USA.

[6]Department of Pediatric Endocrinology, Uniformed Services of the Health Sciences, Bethesda, MD, USA.

Abstract

Purpose—The goal of this study was to analyze the role of somatostatin receptor type 2 (SSTR2) as a molecular target for the imaging and treatment of thyroid cancer (TC) through analysis of SSTR2 expression and its epigenetic modulation and testing tumor uptake of different radiolabeled SSTR2 analogs.

Experimental design—We analyzed SSTR2 expression by immunostaining of 92 TC tissue samples and quantified standard uptake values (SUVmax) of SSTR2 analog ^{68}Ga-DOTATATE by positron emission/computed tomography (PET/CT) imaging in 25 patients with metastatic TC.

[*]**To whom correspondence should be addressed:** Joanna Klubo-Gwiezdzinska, MD, PhD, 10 Center Drive, Building 10, Room 9C-103; Bethesda, MD 20892, Phone 301-496-5052; Cell 301-758-9573; joanna.klubo-gwiezdzinska@nih.gov.

Author contributions:

ST - performed *in vitro* and *in vivo* experiments, wrote the manuscript; BD - performed *in vitro* and *in vivo* experiments, edited the manuscript; CM – performed and analyzed ^{68}Ga-PET/CT images for the patients included in the study, reviewed the manuscript; CC – coordinated patients care, reviewed the manuscript; OJ - provided help with PET imaging in *in vivo* models, analyzed PET scans and biodistribution studies in mice, reviewed the manuscript; HL - helped with mice tail vein injections, reviewed the manuscript; ZW - provided help with PET imaging in *in vivo* models, reviewed the manuscript; DOK. - provided help with PET imaging in *in vivo* models, reviewed the manuscript; XC – synthesized DOTA-EB-TATE, provided help with PET imaging in *in vivo* models, reviewed the manuscript; VV performed IHC on tissue samples and analyzed the results, reviewed the manuscript; JKG designed and supervised the study, analyzed the data, wrote the manuscript.

Conflict of interest:

The authors declare that they have no conflict of interests.

We utilized human TC cell lines characterized by differential SSTR2 expression (TT, BCPAP, FTC133) and rat pancreatic cell line (AR42J) with intrinsically high SSTR2 expression for functional *in vitro* studies. SSTR2-high (AR42J) and SSTR2-low (FTC133) xenograft mouse models were used to test the uptake of radiolabeled SSTR2 analogs and its therapeutic efficacy *in vivo*.

Results—TC had a higher SSTR2 expression than normal thyroid. Hurthle cell TC was characterized by the highest ^{68}Ga-DOTATAE uptake (median SUVmax 16.5 [7.9–29]) than other types of TC. *In vivo* studies demonstrated that radiolabeled DOTA-EB-TATE, is characterized by significantly higher tumor uptake than DOTA-TATE ($p<0.001$) and DOTA-JR11 ($p<0.001$). Treatment with ^{177}Lu-DOTA-EB-TATE extended survival and reduced tumor size in a mouse model characterized by high SST-analogs uptake (SUVmax 15.16±4.34) but had no effects in a model with low SST-analogs uptake (SUVmax 4.8±0.27).

Conclusion—A novel SST-analog, ^{177}Lu-DOTA-EB-TATE, has the potential to be translated from bench to bedside for the targeted therapy of patients characterized by high uptake of SST-analogs in metastatic lesions.

Introduction

The current treatment regimen for metastatic differentiated thyroid cancer (DTC) includes thyroidectomy followed by radioactive iodine (RAI) therapy, while medullary thyroid cancer (MTC) is routinely treated with surgery and tyrosine kinase inhibitors (TKIs) (1). Unfortunately, 5–22% of patients become refractory to standard therapy, particularly patients with Hurthle cell thyroid cancer (HTC) characterized by low RAI uptake in metastatic lesions (2, 3). Previous studies have reported that the average survival for patients with RAI-refractory DTC is around 2.5–3.5 years and with aggressive metastatic MTC – even shorter 1.75 years (4–6).There is a clear need for improved therapy in these patients.

Somatostatins (SST) are a family of cyclopeptides that are produced by endocrine, gastrointestinal, neuronal and immune cells (7). The metabolically stable SST analogs have been labeled with radionuclides to utilize them in peptide receptor radionuclide therapy (PRRT) (8). Treatment efficacy depends on the expression of somatostatin receptors, among which somatostatin receptor type 2 (SSTR2) is the most commonly expressed on tumor tissues (9). Currently, there are several SST analogs available with varying SSTR2 affinities and tumor retention time, with only two (radiolabeled DOTA-TATE and DOTA-TOC) currently approved by the FDA for the imaging of neuroendocrine tumors (NETs) (10, 11) and one approved for the treatment of gastroenteropancreatic NETs - lutetium (^{177}Lu) labeled DOTA-TATE (12). Moreover, recent studies have shown that an SSTR2 agonist combined with Evans blue analog (DOTA-EB-TATE) is characterized by a higher tumor uptake and residence time *in vivo* in preclinical models and in pilot studies of patients with advanced metastatic NETs (13, 14). Recently synthesized SSTR2 antagonists, such as JR11, although not internalized, are reported to have superior binding affinity and long residence time due to slow dissociation from the receptor (15). JR11 was reported to exert superior binding characteristics and tumor-to-background uptake ratios in preclinical models and in pilot clinical trials in patients with metastatic NETs (16–18).

Interestingly, the NIH case series of patients with NETs revealed incidental uptake of radiolabeled SST analog ^{68}Gallium- (^{68}Ga)-DOTA-TATE in thyroid nodules, among which 21% were found to be malignant (19). However, there are no data on the role of radiolabeled DOTA-EB-TATE and DOTA-JR11 in the diagnosis and treatment of thyroid cancer (TC). Therefore, the goal of this study was to provide a comprehensive analysis of SSTR2 expression and mechanisms of its up-regulation in TC and compare the uptake and therapeutic efficacy of radiolabeled SST analogs, that are characterized by different binding capacity and tumor retention times in preclinical models of SSTR2-positive tumors.

Methods

Analysis of ^{68}Ga-DOTA-TATE uptake in patients with metastatic thyroid cancer

The protocol for human studies was approved by the NIH Institutional Review Board and Radiation Safety Committee. All patients gave written informed consent to participate in the studies which were conducted in accordance with the ethical guidelines outlined in the Declaration of Helsinki, CIOMS, Belmont Report, and U.S. Common Rule. We performed a pilot clinical trial (clinicaltrials.gov identifier NCT00001160) aimed at screening patients with RAI-non-avid metastatic DTC and MTC for the presence of SSTR2 expression by imaging with ^{68}Ga-DOTA-TATE positron emission tomography/computed tomography (PET/CT). Each patient received 5mCi of ^{68}Ga-DOTA-TATE intravenously followed by PET/CT imaging per standard protocol. Any lesion demonstrating activity higher than the physiologic uptake of the involved organ was considered a “true” lesion unless correlative anatomic imaging suggested non-malignant or alternative pathology (20). Two investigators (CM, JKG) analyzed the images and obtained maximum and mean standard uptake values (SUV) for up to 6 lesions in each patient.

Cell culture

The human TC cell lines gifted from Dr Electron Kebebew from Stanford University or purchased from University of Colorado Cancer Center or ATCC were used in this study: follicular TC - FTC133, papillary TC - BCPAP, TPC1; MTC - TT; anaplastic TC THJ16T, THJ29T, 8505C, OCUT2, KAT18, SW1736 and C643 (ATC); and HTC - XTC1. A rat pancreatic cell line, AR42J, with intrinsically high SSTR2 expression, was used as a positive control for SST analog uptake studies (13). The cells were authenticated by short tandem repeat (STR) analysis and contamination was excluded via IMPACT II PCR analysis.

The cells were grown in the standard media, supplemented with 10% FBS (ThermoFisher Scientific) for human cell lines and 20% for a rat AR42J cell line, as well as with 10 U/mL penicillin-streptomycin (Gibco) and 0.25 μg/mL amphotericin B (Gibco). For treatment (72h), valproic acid (VAC, Sigma Aldrich, PHR1061) was added to the culture medium at a final concentration of 2 mM or 4 mM, while tacedinaline (Sigma Aldrich, C0621) and decitabine (Sigma Aldrich, A3656) at final concentration of 500 ng/mL and 75 ng/mL, respectively which corresponds to their therapeutic serum concentrations (21).

RNA extraction and real-time reverse transcription PCR

For mRNA analysis, cells were seeded in 6-well plates and total RNA was isolated from the cells using RNeasy Mini Kit (Qiagen). RNA was quantified using Nanodrop (manufacturer) and 1 μg of RNA was used to synthesize cDNA using the iScript cDNA synthesis kit (Biorad). The relative gene expression was analyzed using iQ SYBR Green Supermix (Bio-Rad) on a StepOnePlus Real-Time PCR Detection System (Applied Biosystems). We used commercially available primers for the analysis of SSTR2 (Hs_SSTR2_1_SG QuantiTect Primer Assay; Rn_Sstr2_1_SG QuantiTect Primer Assay) and β-Actin (Hs_ACTB_2_SG QuantiTect Primer Assay; Rn_Actb_1_SG QuantiTect Primer Assay) expression. The relative gene expression was normalized to β-actin and calculated using the $2^{-\Delta\Delta Ct}$ method.

Western blotting

Cells were seeded in a 10cm culture plate and lysed using mammalian protein extraction reagent (M-PER, ThermoFisher Scientific) as per manufacturer instructions. To increase the protein concentration, Amicon centrifugal filters (Millipore) were used. The protein concentration was determined using the DC™ Protein Assay Kit II. The samples were loaded onto 4–12% SDS-PAGE gel (Novex) (30–50 μg/lane) and transferred onto a PVDF membrane using a Trans-blot turbo system (Biorad). The membranes were blocked with 3% BSA and prepared in PBST for 1h at room temperature. The membranes were incubated overnight at 4^{o}C with a primary antibody against SSTR2 (1:400, R&D systems, MAB4224), acetylated histone 3 (1:500, Millipore, 06–599) or acetylated histone 4 (1:500, Millipore, 06–598), GAPDH (1:1000; Invitrogen; MA5–15738) and β-actin (1:1000, Santa Cruz Biotechnology, sc-47778). The membranes were washed three times with PBST followed by incubation with either anti-mouse or anti-rabbit secondary antibody for 1h at room temperature. The membranes were finally washed three times with PBST and imaged using ECL (Azure Biosystems) and an imaging system (Bio-Rad).

Cell surface expression of SSTR2

To analyze the membranous expression of SSTR2, cells were harvested, washed and counted. The cells were then resuspended in ice-cold PBS containing 10% fetal calf serum and 1% sodium azide at a concentration of 2×10^{6} cells/mL. For each sample, 200μL of this cell suspension was used and 2 μg of SSTR2 antibody was added and incubated for 1h at room temperature. Following incubation, the cells were washed three times with ice-cold PBS by centrifugation at 1000rpm for 5 min. After washings, cells were incubated with an Alexa Fluor 680 labeled secondary antibody (4μg), which was prepared in 3% BSA in PBS. The cells were incubated for 30 min at room temperature in the dark and washed three times, followed by resuspension in ice-cold PBS containing 3% BSA and 1% sodium azide. The cells were immediately analyzed by flow cytometer (LSR II, BD Biosciences) for SSTR2 membranous expression. To avoid any detection of intracellular SSTR2, cell permeabilization was avoided.

Immunohistochemistry

Immunostaining was performed on commercially available human TC tissue microarray slides (US Biomax Inc., Rockville, MD) and on formalin-fixed paraffin-embedded tissue

samples from thyroidectomized patients (MTC, HTC) and animal TC models. Sections were dewaxed, soaked in alcohol, and then microwave treated in antigen unmasking solution (Vector Labs, Burlingame, CA, USA) for 10 min. Endogenous peroxidase activity was quenched by incubation in 3% hydrogen peroxide. Sections were then incubated for 10 min in a working solution of blocking serum and incubated at 4°C overnight with anti-SSTR2 antibody (Abcam, Cambridge, MA, cat# ab9550, dilution 1/100). Immunostaining was performed using the Vectastain Universal Quick Kit (Vector Laboratories Inc., Burlington, CA, USA) as per manufacturer instructions. Sections were incubated with biotinylated secondary antibody for 10 min and in streptavidin/peroxidase complex working solution for 10 min. Peroxidase staining was revealed with the ImmPact DAB peroxidase substrate kit (Vector Labs). Sections were counterstained with hematoxylin and mounted. The antiserum was omitted in the negative control. The results of staining were interpreted and scored independently by two investigators (VV and JKG). The intensity of staining was scored as 0 (negative staining) and 1 (positive - intensity similar to those obtained in positive control). The quantitative data from the assessment of relative percentage of immunopositive cells in thyroid tissue samples were calculated as 0–no staining, 1–positive staining in <25% of cells, 2–positive staining in 25–50% of cells, 3–positive staining in >50% of cells. The final immunoscore was calculated by multiplying each score (22).

Chromatin immunoprecipitation (ChIP) assay

Cells were cultured in 150mm cell culture dishes. The ChIP assay was performed using the ChIP-IT® Express Enzymatic kit (Active Motif, 53009) as per the manufacturer instructions. The chromatin was sheared using the ChIP-IT Express Enzymatic kit (Active motif, 53035). We used Histone H3ac (pan-acetyl) antibody (Active motif, 39139), Histone H4ac (pan-acetyl) antibody (Active motif, 39243) and isotype IgG control for immunoprecipitation. The immunoprecipitated DNA was analyzed by real-time PCR for H3 and H4 acetylation at the SSTR2 promoter by using primers directed against the human and rat SSTR2 gene promoter. The sequence of human SSTR2 primers are: forward primer-GAAGGAAGGAAGGAAGAA; reverse primer–GGATGAAGTCATTGATGTC, while the sequence of rat SSTR2 primers are: forward primer–CCCGGGACTGGTCCGTGGTA; reverse primer–CAGCTGGTGTGGCGACTGGG. ChIP data were normalized to the input DNA and were analyzed as fold-enrichment relative to isotype control antibody.

Mice models

The animal protocol for the experiments was approved by the NIDDK Animal Care and Use Committee. Eight to ten weeks old athymic nude mice and NOD.Cg-Prkdcscid Il2rgtm1Wjl/SzJ mice (Jackson Laboratory, Bar Harbor, ME) were used to create subcutaneous xenograft and metastatic mouse models, respectively. For the metastatic model, the mice received a tail vein injection of FTC133 (160,000 cells) containing a linearized pGL4.51[luc2/CMV/Neo] vector (23). The tumor burden was monitored weekly in the mice using the IVIS Lumina In Vivo Imaging System (PerkinElmer) by injecting them with luciferin (150mg Luciferin/kg body weight, PerkinElmer) 10 min before imaging. For the subcutaneous xenograft model, athymic nude mice were injected subcutaneously with FTC133, BCPAP, TT, or AR42J (500,000 cells). The tumor burden was monitored regularly by using a Vernier caliper. The mice were euthanized if the tumors exceeded 2cm

in diameter, impeded movement, or if there were signs of breathing difficulty at any point in the study. The mice were grouped into control and treatment groups based on weight, gender and tumor burden. The mice were then treated with either VAC (300 μg/kg; Sigma Aldrich, P4543), decitabine (1 mg/kg), or saline (placebo) *via* intraperitoneal injections daily for 10 days followed by PET imaging or radionuclide therapy studies (Supplemental Figure 8).

PET imaging and biodistribution studies

PET imaging was performed in the metastatic mice model at 4–5 weeks post-inoculation when the average luminescence in the metastatic areas was in the range of 10^7-10^8. For the subcutaneous xenograft mice model, PET imaging was performed when the tumor sized exceeded 1 cm. The FTC133 and AR42J formed 1–2 cm tumors within 2 weeks post-inoculation, while BCPAP - in 3–4 weeks and TT – in 4–5 weeks. Each mouse received a dose of ~100 μCi of each radiolabeled SST analog (^{68}Ga-DOTA-TATE, ^{68}Ga-DOTA-JR11, ^{86}Y-DOTA-EB-TATE) consecutively *via* tail vein injection. DOTA-TATE (TATE supplied by CSBio) and DOTA-JR11 (JR11 provided by IPSEN®), as agents characterized by a short half-life, were labeled with ^{68}Ga with a half-life of 67.7 min. DOTA-EB-TATE (EB-TATE patented by NIH and licensed by Molecular Targeting Technologies Inc.), an agent with a long half-life in the blood due to a reversible binding to albumin[25], required radiolabeling with ^{86}Y, since this isotope is characterized by a longer half-life of 14.7 h. These pharmacokinetics and pharmacodynamics formed the rationale for the particular order of consecutive injections for each mouse with ^{68}Ga-DOTA-TATE and ^{68}Ga-DOTA-JR11, injected 4 h apart (~4 half-lives apart), followed by DOTA-EB-TATE as the last SST analog in all mice (Supplemental Figure 8A). Randomization to injection of the DOTA-EB-TATE as the first agent is futile since it would necessitate performing the remaining PET/CTs after approximately 4 days (~4 half-lives). Significant tumor growth could take place during this delay, rendering the imaging results incomparable. The static PET imaging for ^{68}Ga-DOTA-TATE and ^{68}Ga-DOTA-JR11 was done at 60 min post-injection, while for ^{86}Y-DOTA-EB-TATE imaging was performed at 16–24 h post-injection per the previously published pharmacokinetic and pharmacodynamic studies (13, 24). The PET scans were acquired on Inveon (Siemens) scanners. The PET images were analyzed using ASIPro (Siemens) to plot regions of interest (ROI) and calculate standard uptake value (SUV). The SUV was corrected for injected radioactivity dose, decay, branching, and mouse weight. After the last scan, mice were euthanized and tumor, heart, lungs, liver, spleen, and kidneys were collected to perform biodistribution studies. The counts per minute (CPM) readings were normalized by the weight of the tissues and biodistribution data are presented as percentages of the injected dose per gram of tissue (%ID/g).

PRRT

To evaluate therapeutic efficacy, the SST analogs were labeled with the therapeutic radionuclide ^{177}Lu. The FTC133 and AR42J tumor mice models were pretreated with either placebo or VAC, with a goal of inducing SSTR2 expression in the tumors of VAC-treated animals. The mice were divided into control and VAC groups based on their body weight and gender. Two weeks post-inoculation, the mice in control and VAC groups were subdivided into the following groups: 1) Control placebo-treated mice receiving ^{177}Lu-DOTA-EB-TATE (500 μCi); 2) Control placebo-treated mice receiving saline; 3)

VAC-treated mice receiving ^{177}Lu-DOTA-EB-TATE (500 μCi); and 4) VAC-treated mice receiving saline (Supplemental Figure 8B). All mice received two doses of either ^{177}Lu-DOTA-EB-TATE or saline a week-apart. The tumor burden in each mouse was monitored twice a week and living mice were euthanized 60 days post-first ^{177}Lu-DOTA-EB-TATE injection. The tumor burden was calculated using the formula: tumor volume = (width^2 × length)/2.

Subsequently, to compare the therapeutic effects of different SST analogs, we utilized mice with AR42J tumors characterized by the highest SST analogs uptake. Prior to therapy initiation, the mice were divided into three groups based on their tumor volume, gender and body weight as follows: 1) ^{177}Lu-DOTA-TATE (500 μCi); 2) ^{177}Lu-DOTA-JR11 (500 μCi); and 3) ^{177}Lu-DOTA-EB-TATE (500 μCi) (Supplemental Figure 8C). All mice received their first dose two weeks post-inoculation and the second dose was given seven days later. The effect of the therapy was analyzed by obtaining tumor measurements twice a week. Living mice were euthanized 24 days post-first ^{177}Lu-labeled SST analog injection.

Statistical Analysis

GraphPad Prism 8.1 software was used for data analysis. A two-tailed unpaired Student's t-test was used for comparison between two groups. One-way ANOVA with posthoc Tukey's test was used for comparison between more than two groups. Data are presented as mean±S.D or mean±SEM for normally distributed data and median with [25–75 IQR range] for skewed data. A P-value of <0.05 was considered significant.

Results

SSTR2 is overexpressed in TC compared with normal thyroid tissue

RNA sequencing data available in The Cancer Genome Atlas (TCGA) database was analyzed for 507 patients with PTC (25), demonstrating that SSTR2 is expressed in all PTC stages and subtypes (Supplemental Figure 1A, B). This included 65 paired samples of tumor versus normal thyroid tissues, derived from the same patients, which demonstrated significantly higher SSTR2 expression in tumor tissue samples compared to the paired normal thyroid tissues (log fold change 0.6, p=0.03).

Immunostaining on 92 human tissue samples – 84 TC tissue samples (39 PTC, 19 FTC, 6 poorly differentiated cancers, 16 MTC and 4 HTC), and 8 normal thyroid tissues – showed high SSTR2 protein expression (IHC score 2, 3) in 51.4% (35/68) of TC samples of epithelial origin and 43.8% (7/16) of MTC samples. There was no significant expression in the normal thyroid samples (Figure 1A, Supplemental Table 1).

The highest ^{68}Ga-DOTA-TATE uptake is observed in metastatic HTC patients

To analyze the presence of SSTR2 in TC metastases, ^{68}Ga-DOTA-TATE PET/CT was performed in patients with RAI non-avid metastatic DTC and MTC. Among 25 enrolled patients, aged 52.2 ± 13 years old at the study enrollment and 40±15 at TC diagnosis, 13/25 (52%) were females, 5 presented with HTC, 8 with MTC and 12 with PTC. ^{68}Ga-DOTA-TATE PET/CT was positive in 20/25 (80%) patients. The highest uptake was observed

in patients with HTC (median SUVmax 16.5 [7.9–29]) compared with MTC patients characterized by low-to-moderate SUV max (median 4.3 [3.2–9.5], p=0.019) and PTC patients with median SUVmax of 5.4 [3.8–7.8], p=0.007 (Figure 1B). Two MTC and 3 PTC patients had no evident uptake above the background, suggesting a lack of, or very low, SSTR2 expression in their metastatic lesions. The PET/CT images demonstrating high ^{68}Ga-DOTA-TATE uptake are depicted in Figure 1C (HTC), D (PTC), and E (MTC). Since the high therapeutic efficacy of PRRT in NETs has been associated with tumors characterized by SUVmax>13–15 (26, 27), we further showed that SUVmax >15 was observed in at least one metastatic lesion in 7/25 (28%) enrolled patients. It was observed in 4/5 (80%) patients with metastatic HTC, 1/12 (8.3%) patients with metastatic PTC and 2/8 (25%) patients with metastatic MTC (Supplemental Table 2).

Given only low-to-moderate ^{68}Ga-DOTA-TATE uptake in a majority of PTC and MTC patients, functional *in vitro* and *in vivo* studies were performed to test if SSTR2 expression could be significantly and safely upregulated and if radiolabeled SST analogs, besides DOTA-TATE, might be associated with higher tumor uptake.

TC cell lines are characterized by variable SSTR2 expression that can be epigenetically upregulated

Several TC cell lines were screened for the presence of SSTR2 by RT-PCR (Supplemental Figure 1C). The TC cell lines TT, FTC133, and BCPAP were chosen for subsequent functional *in vitro* and *in vivo* studies based on differential SSTR2 expression, histologic origin and ability to form tumors *in vivo.* (Supplemental Figure 1E).

Since the TC cell lines had low-to-moderate SSTR2 expression, it was analyzed whether SSTR2 could be upregulated in an *in vitro* model. SSTR2 is an epigenetically regulated gene and, therefore, we utilized epigenetic modifiers – histone deacetylase [HDAC] inhibitors valproic acid (VAC) and tacedinaline (TAC) and DNA methyltransferase (DNMT) inhibitor-decitabine (DEC) (21). VAC was observed to be a more potent inducer of SSTR2 expression in thyroid cancer cells in comparison to TAC and DEC (Supplemental Figure 2 A, B). Treatment with 2 mM or 4 mM VAC for 72 h significantly upregulated SSTR2 expression in FTC133, BCPAP and TT cells (Figure 2 A, B, C, F, G, H, Supplemental Figure 1 F, G, H, I, K) as well as in the .AR42J cell line (Figure 2 K, L, M, Supplemental Figure 1 J). Flow cytometry demonstrated an increased membranous SSTR2 expression in examined cell lines (Figure 2 B, G, L). VAC treatment resulted in growth inhibition by promoting cell cycle arrest (Supplemental Figure 3 A–L).

Since VAC is an HDAC inhibitor, the effects of VAC on the acetylation of histones 3 (H3ac) and 4 (H4ac) were analyzed. As indicated in Figure 2 D, I, N, we observed an increase in H3ac and H4ac in VAC treated FTC133, BCPAP, and AR42J cells. To further identify if VAC-mediated upregulation of SSTR2 expression is caused by an increase in H3 or H4 acetylation at the SSTR2 promoter, ChIP assays were performed. VAC treatment in BCPAP and AR42J cells resulted in a significant increase in both H3ac (1.9 fold-BCPAP, $p<0.001$; 2.8 fold-AR42J, $p<0.001$) and H4ac (2.9 fold-BCPAP, $p<0.001$; 2.7 fold-AR42J, $p<0.01$) (Figure 2 J, O). In contrast, in FTC133 cells, H4 acetylation was increased by 2.4-fold ($p<0.001$) at the SSTR2 promoter, while H3 acetylation was slightly, but

significantly reduced ($p<0.05$) (Figure 2E). Overall, our results indicate that VAC treatment is associated withincreasedSSTR2 expression in TC cells independent of baseline expression levels. Higher SSTR2 protein expression in VAC-treated cells is associated with increased acetylation of H3 and/or H4 at the SSTR2 promoter.

^{86}Y-DOTA-EB-TATE is a superior SST analog in the imaging of SSTR2 expressing tumors

The uptake of the radiolabeled SST analogs in FTC133, BCPAP, TT, and AR42J subcutaneous xenograft models was analyzed. Irrespective of the cell lines, ^{86}Y-DOTA-EB-TATE showed the highest tumor uptake in all mice models in comparison to ^{68}Ga-DOTA-TATE and ^{68}Ga-DOTA-JR11 (Figure 3 A, C, D, E, Table 1).

The uptake of ^{68}Ga-DOTA-TATE and ^{68}Ga-DOTA-JR11 was similar in all mice models (Table1). Tumors derived from AR42J cells (high SSTR2 expression) showed the highest uptake among all SST analogs in comparison to FTC133, BCPAP and MTC (TT) mice models ($p<0.001$) (Figure 3F, Table 1).

In addition to the subcutaneous mice model, the uptake of three SST analogs was examined in a metastatic FTC133 mice model. Similar to the subcutaneous mouse model, ^{86}Y-DOTA-EB-TATE had the highest uptake in the metastatic lesions in comparison to ^{68}Ga-DOTA-TATE ($p<0.001$) and ^{68}Ga-DOTA-JR11 ($p<0.001$), respectively (Figure 3B).

We next evaluated if VAC treatment improved the uptake of SST analogs in the subcutaneous and metastatic mice models. Irrespective of the model, no significant effect from VAC treatment was observed on the uptake of the SST analogs (Supplemental Figure 4 A, B, C, D). However, IHC staining did reveal higher cytoplasmic SSTR2 expression in tumor tissues derived from mice exposed to VAC compared with placebo in FTC133 ($p=0.023$) and AR42J ($p=0.016$) models (Supplemental Table 3). Similar to VAC, decitabine treatment did not improve the uptake of ^{86}Y-DOTA-EB-TATE in FTC133 and AR42J subcutaneous mice models as indicated by PET scans (Supplemental Figure 5 A, B).

The alternative to the upregulation of SSTR2 *in vivo* is to utilize SST analogs possessing the highest binding affinity and diagnostic and therapeutic activity. Significantly enhanced tumor uptake could be obtained by using the SST analog ^{86}Y-DOTA-EB-TATE compared with ^{68}Ga-DOTA-TATE ($p<0.001$) and ^{68}Ga-DOTA-JR11 ($p<0.001$).

High-SSTR2-expressing tumors are characterized by enhanced uptake of an SST analog

To determine and compare the uptake of radiolabeled SST analog by normal body organs and tumor tissue, biodistribution studies were performed on FTC133 and AR42J tumor-bearing mice after ^{86}Y-DOTA-EB-TATE scans. In FTC133 mice, the uptake by tumor tissue (5.8 ± 0.8 %ID/g) was comparable to the spleen (5.1 ± 3.5 %ID/g; $p=0.7$), while the liver (4.24 ± 0.43 %ID/g; $p<0.01$) and heart (3.76 ± 0.7 %ID/g; $p<0.01$) had significantly lower uptake compared to tumor tissue. In contrast, uptake by the kidneys (11.6 ± 1.1 %ID/g; $p<0.001$) and lungs (8.5 ± 1.4 %ID/g; $p<0.01$) was significantly higher than FTC133 tumors (Figure 4A). In AR42J tumor-bearing mice, tumor uptake (19.13 ± 8.8 %ID/g) was superior to the uptake by the liver (2.4 ± 0.56 %ID/g; $p<0.01$), kidneys (6.9 ± 1.5 %ID/g; $p<0.05$), spleen (2.2 ± 0.8 %ID/g; $p<0.01$), heart (2.4 ± 0.36 %ID/g; $p<0.01$) and lungs

(5.4 ± 1 %ID/g; $p<0.05$) (Figure 4D). Similar to PET imaging, biodistribution analysis also revealed superior uptake by AR42J tumors (3.3-fold higher; $p<0.05$) in comparison to FTC133 tumors. Moreover, as expected, higher uptake of ^{86}Y-DOTA-EB-TATE by AR42J tumors was associated with relatively reduced uptake by normal organs in comparison to the FTC133 mice model. Neither VAC nor DEC treatment resulted in any significant difference in the uptake of ^{86}Y-DOTA-EB-TATE within the tumor and normal tissues in comparison with the control mice (Supplemental Figure 6 A, B, C, D).

^{177}Lu-DOTA-EB-TATE therapy promotes tumor regression and improves disease-specific survival in high-SSTR2-expressing tumors

Since DOTA-EB-TATE had the highest uptake in tumor tissues, therapeutic efficacy of this radiolabeled with ^{177}Lu (half-life 6.7 days) analog was tested in high-SSTR2-expressing (AR42J) and low-SSTR2-expressing tumors (FTC133). After receiving the first dose of ^{177}Lu-DOTA-EB-TATE, AR42J tumors were stabilized and did not progress further in size. After receiving a second dose one week later, these mice showed a decline in tumor growth. In contrast, the tumors of placebo-treated mice continued to progress, and the mice had to be euthanized within 14 days (Figure 4 E, F). The disease-specific survival of the mice that received ^{177}Lu-DOTA-EB-TATE therapy was significantly higher than the control group ($p<0.001$). In contrast, the low-SSTR2-expressing FTC133 tumors did not respond to the ^{177}Lu-DOTA-EB-TATE treatment. (Figure 4 B, C). VAC pretreatment did not improve the efficacy of ^{177}Lu-DOTA-EB-TATE in either AR42J or FTC133 mice models (Supplemental Figure 7 A, B).

The therapeutic efficacy of all three SST analogs was compared in the AR42J mice model. Consistent with the observed higher tumor uptake on imaging, ^{177}Lu-DOTA-EB-TATE-treated mice responded to treatment with an overall 87 ± 13% reduction in the tumor volume after two weeks (Figure 5 A, B). In contrast, mice treated with ^{177}Lu-DOTA-TATE and ^{177}Lu-DOTA-JR11 showed continued tumor progression and the mice had to be euthanized within 10 days after the starting therapy (Figure 6 A, B). The disease-specific survival in the ^{177}Lu-DOTA-EB-TATE treated mice (24 ± 0 days) was significantly longer compared with ^{177}Lu-DOTA-TATE (7.7 ± 2.6 days, $p<0.001$) and ^{177}Lu-DOTA-JR11 (6.3 ± 3 days, $p<0.001$) treated mice (Figure 5C). There was no difference in disease-specific survival between ^{177}Lu-DOTA-TATE and ^{177}Lu-DOTA-JR11-treated mice ($p=0.3$) (Figure 5C). Thus, ^{177}Lu-DOTA-EB-TATE is characterized by superior therapeutic efficacy in the management of tumors with high SSTR2 expression. None of the radiolabeled SST analogs is effective in tumors with low-to-moderate SSTR2 expression.

Discussion

We demonstrated that SSTR2 may serve as a molecular target in the diagnosis and treatment of a subset of TC patients. First, we showed that patients with HTC are characterized by high ^{68}Ga-DOTA-TATE uptake. As SUVmax of >13–15 has been associated with improved objective response rate and extended progression free survival in patients with NETs, the median SUVmax of 16.5 [7.9–29] observed in HTC patients suggests that PRRT might be beneficial in these patients, which are currently lacking effective therapeutic options

(26–29). Further supporting this observation is our *in vivo* AR42J model characterized by average EB-TATE SUVmax of 15.16±4.34 in the tumor tissue, that responded to therapy with ^{177}Lu-EB-TATE with a significant reduction in tumor size and extended survival. In contrast, FTC133 *in vivo* model with a low radiolabeled analogs SUVmax of 4.8±0.27 did not respond to PRRT.

At present, there are a few small-scale studies showing promising results for the treatment of RAI-non-avid TC patients with radiolabeled SST analogs (30–32). In a study of 16 patients with RAI-non-avid progressive TC (8 DTC, 8 MTC), treatment with ^{90}Yttrium and/or ^{177}Lu labeled DOTA-TATE resulted in mean overall survival (OS) of 4.2 years (95% CI, range 2.9–5.5) and median progression-free survival (PFS) of 25 months after initial PRRT (30). *Versari* et al. documented positive ^{68}Gallium-DOTATOC uptake in 24 out of 41 patients with progressive RAI-negative DTC and 11 patients treated with PRRT (^{90}Y-DOTATOC), showing an objective response rate of 63% with a response duration of 3.5–11.5 months (32). However, PRRT utilizing ^{90}Y has been associated with nephrotoxicity, which could be decreased by utilizing ^{177}Lu for radiolabeling (33). In contrary to these studies, ^{177}Lu-DOTA-TATE therapy of five patients with radioiodine-refractory DTC showed heterogeneous response despite good ^{68}Ga-DOTA-TATE uptake in the pre-therapeutic PET scan (34). In our study, we showed that only a subset of TC patients has high uptake of radiolabeled SST analogs and may potentially benefit from PRRT therapy. Therefore, we investigated potential ways to upregulate SSTR2 in preclinical models and tested SST analogs characterized by different binding capacities and pharmacokinetics.

SSTR2 expression has been shown to be regulated by epigenetic modulators (21, 35–38). We screened three epigenetic regulators of SSTR2 expression and utilized the most potent among them- HDAC inhibitor VAC, which is commonly used for the treatment of epilepsy and shown to have an excellent safety profile (39). We showed that VAC increases SSTR2 expression in TC cell lines *in vitro,* which is associated with increased H3 and H4 acetylation at the SSTR2 promoter region. Unfortunately, we did not observe a significant VAC-induced increase in the uptake of SST analogs *in vivo*. Although VAC upregulated SSTR2 expression in the tumor tissues of the subcutaneous FTC133 and AR42J models, this increase in expression might be insufficient and characterized by a lack of increased localization of SSTR2 on the cell surface. In the future, it will be interesting to test more tumor-specific epigenetic regulators to improve SSTR2 expression on the cancer cell surface.

Our study is the first to test novel SST analogs DOTA-EB-TATE and DOTA-JR11 in TC, demonstrating that DOTA-EB-TATE is a superior SST agonist. We compared the SUV of the three analogs in each mouse serving as their own control and observed that DOTA-EB-TATE is characterized by enhanced SUV compared with DOTA-TATE and DOTA-JR11. We also compared the therapeutic efficacy of ^{177}Lu-labeled DOTA-TATE, DOTA-JR11, and DOTA-EB-TATE, documenting the superiority of the latter in the mouse model characterized by high SSTR2 expression. There are several studies that suggested the superiority of SST antagonists over SST agonists (16, 40, 41). In our study, no significant difference was observed in the uptake of octreotate (TATE-agonist) vs JR11 (antagonist) linked to the same

chelator (DOTA) in the tested mice models. However, attachment of Evans-Blue moiety to octreotate improved the uptake significantly. The addition of Evans-Blue moiety to the octreotate significantly improved its pharmacokinetics, as indicated by the increased half-life in the blood, lower clearance rate, and better tumor to organ uptake ratio (13, 14). In a recent study performed on 33 patients with metastatic NETs, ^{177}Lu-DOTA-EB-TATE was observed to be more effective than similar dose of ^{177}Lu-DOTA-TATE (42). However, the study endpoint was a change in SUV before and after treatment, so there was no data on the effects on standardized hard endpoints such as response rate by RECIST criteria, progression-free and overall survival. A possible concern regarding the use of DOTA-EB-TATE is that it's enhanced binding to the albumin and slow clearance rate will not only expose the tumor tissues but also the healthy organs to the higher radiation doses. A study analyzing the safety profile of this agent reported that in comparison to ^{177}Lu-DOTA-TATE, the effective dose of ^{177}Lu-DOTA-EB-TATE was significantly higher in the kidneys and red bone marrow of the metastatic NET patients (14). Although the small-scale pilot studies performed on patients with metastatic NETs showed that ^{177}Lu-DOTA-EB-TATE is well tolerated by the patients at low doses without causing any significant hematotoxicity or nephrotoxicity (42, 43), more studies are necessary to understand the short- and long-term toxicity profile of this agent.

The major strength of our study is its translational relevance, as therapeutic efficacy of PRRT has been proven only for the model characterized by a high SSTR2 analogs uptake. It suggests that the tumors characterized by a high SUVmax, within 15.16±4.34 range, may respond to PRRT using ^{177}Lu-DOTA-EB-TATE, while the uptake within SUV max of 4.8±0.27 is likely not going to translate into clinical efficacy.

Our study had a few limitations. We utilized non-TC AR42J xenografts to model a high SUV of SST-analogs, resembling SUVmax observed in our clinical trial in HTC patients, as all screened TC cell lines were characterized by low to moderate uptake of SST analogs *in vivo*. Nonetheless, testing radiolabeled SST analogs in models with differential SSTR2 expression levels revealed that the therapeutic efficacy of PRRT is achieved only in tumors with high SST-analogs uptake.

In conclusion, our preclinical data document that DOTA-EB-TATE is a superior analog over DOTA-TATE and DOTA-JR11 for the imaging and treatment of SSTR2-high-expressing tumors. A high ^{68}Ga-DOTA-TATE uptake observed in metastatic HTC makes these patients, who lack alternative treatment options, ideal candidates for PRRT therapy. Our study forms a basis for a clinical trial testing the diagnostic and therapeutic efficacy of ^{177}Lu-DOTA-EB-TATE in patients with tumors characterized by high SST-analogs uptake.

Supplementary Material

Refer to Web version on PubMed Central for supplementary material.

Acknowledgments:

This work was supported by NIH/NIDDK Intramural Funding ZIA DK 07513803.

We thank our patients for participation in the study.

We thank IPSEN® for providing DOTA-JR11 for the animal studies.

Special thanks to Dr. Peter Herscovitch – Chief of Positron Emission Tomography for supporting the clinical part of the study.

Special thanks to Drs. Hongxiu Luo and Shirisha Avadhanula for seeing and coordinating care for a subset of study participants.

Special thanks to flow cytometry core facility, National Heart, Lung, and Blood Institute (NHLBI), NIH for their help with flow cytometer experiments.

We thank Drs. Lee S. Weinstein and Sunita Agarwal for a critical review of the paper.

We thank Sungyoung Auh for the statistical analysis of the data in relation to a reviewer's comment.

References:

1. Wells SA, Jr., Asa SL, Dralle H, Elisei R, Evans DB, Gagel RF, et al. Revised American Thyroid Association guidelines for the management of medullary thyroid carcinoma. Thyroid 2015;25(6):567–610. [PubMed: 25810047]
2. Dadu R, and Cabanillas ME. Optimizing therapy for radioactive iodine-refractory differentiated thyroid cancer: current state of the art and future directions. Minerva Endocrinol 2012;37(4):335–56. [PubMed: 23235190]
3. Besic N, Vidergar-Kralj B, Frkovic-Grazio S, Movrin-Stanovnik T, and Auersperg M. The role of radioactive iodine in the treatment of Hurthle cell carcinoma of the thyroid. Thyroid : official journal of the American Thyroid Association 2003;13(6):577–84. [PubMed: 12930602]
4. Durante C, Haddy N, Baudin E, Leboulleux S, Hartl D, Travagli JP, et al. Long-term outcome of 444 patients with distant metastases from papillary and follicular thyroid carcinoma: benefits and limits of radioiodine therapy. J Clin Endocrinol Metab 2006;91(8):2892–9. [PubMed: 16684830]
5. Robbins RJ, Wan Q, Grewal RK, Reibke R, Gonen M, Strauss HW, et al. Real-time prognosis for metastatic thyroid carcinoma based on 2-[18F]fluoro-2-deoxy-D-glucose-positron emission tomography scanning. J Clin Endocrinol Metab 2006;91(2):498–505. [PubMed: 16303836]
6. Frank-Raue K, Machens A, Leidig-Bruckner G, Rondot S, Haag C, Schulze E, et al. Prevalence and clinical spectrum of nonsecretory medullary thyroid carcinoma in a series of 839 patients with sporadic medullary thyroid carcinoma. Thyroid : official journal of the American Thyroid Association 2013;23(3):294–300. [PubMed: 22946486]
7. Weckbecker G, Lewis I, Albert R, Schmid HA, Hoyer D, and Bruns C. Opportunities in somatostatin research: biological, chemical and therapeutic aspects. Nat Rev Drug Discov 2003;2(12):999–1017. [PubMed: 14654798]
8. De Jong M, Valkema R, Jamar F, Kvols LK, Kwekkeboom DJ, Breeman WA, et al. Somatostatin receptor-targeted radionuclide therapy of tumors: preclinical and clinical findings. Semin Nucl Med 2002;32(2):133–40. [PubMed: 11965608]
9. Sun LC, and Coy DH. Somatostatin receptor-targeted anti-cancer therapy. Curr Drug Deliv 2011;8(1):2–10. [PubMed: 21034425]
10. Hennrich U, and Benesova M. [(68)Ga]Ga-DOTA-TOC: The First FDA-Approved (68)Ga-Radiopharmaceutical for PET Imaging. Pharmaceuticals (Basel) 2020;13(3). [PubMed: 33374474]
11. Raj N, and Reidy-Lagunes D. The Role of 68Ga-DOTATATE Positron Emission Tomography/Computed Tomography in Well-Differentiated Neuroendocrine Tumors: A Case-Based Approach Illustrates Potential Benefits and Challenges. Pancreas 2018;47(1):1–5. [PubMed: 29232339]
12. Maqsood MH, Tameez Ud Din A, and Khan AH. Neuroendocrine Tumor Therapy with Lutetium-177: A Literature Review. Cureus 2019;11(1):e3986. [PubMed: 30972265]
13. Tian R, Jacobson O, Niu G, Kiesewetter DO, Wang Z, Zhu G, et al. Evans Blue Attachment Enhances Somatostatin Receptor Subtype-2 Imaging and Radiotherapy. Theranostics 2018;8(3):735–45. [PubMed: 29344302]
14. Zhang J, Wang H, Jacobson O, Cheng Y, Niu G, Li F, et al. Safety, Pharmacokinetics, and Dosimetry of a Long-Acting Radiolabeled Somatostatin Analog (177)Lu-DOTA-EB-TATE in

Patients with Advanced Metastatic Neuroendocrine Tumors. Journal of nuclear medicine : official publication, Society of Nuclear Medicine 2018;59(11):1699–705. [PubMed: 29653971]

15. Fani M, Nicolas GP, and Wild D. Somatostatin Receptor Antagonists for Imaging and Therapy. Journal of nuclear medicine : official publication, Society of Nuclear Medicine 2017;58(Suppl 2):61s–6s. [PubMed: 28864614]
16. Ginj M, Zhang H, Waser B, Cescato R, Wild D, Wang X, et al. Radiolabeled somatostatin receptor antagonists are preferable to agonists for in vivo peptide receptor targeting of tumors. Proc Natl Acad Sci U S A 2006;103(44):16436–41. [PubMed: 17056720]
17. Dalm SU, Nonnekens J, Doeswijk GN, de Blois E, van Gent DC, Konijnenberg MW, et al. Comparison of the Therapeutic Response to Treatment with a 177Lu-Labeled Somatostatin Receptor Agonist and Antagonist in Preclinical Models. Journal of nuclear medicine : official publication, Society of Nuclear Medicine 2016;57(2):260–5. [PubMed: 26514177]
18. Nicolas GP, Schreiter N, Kaul F, Uiters J, Bouterfa H, Kaufmann J, et al. Sensitivity Comparison of (68)Ga-OPS202 and (68)Ga-DOTATOC PET/CT in Patients with Gastroenteropancreatic Neuroendocrine Tumors: A Prospective Phase II Imaging Study. Journal of nuclear medicine : official publication, Society of Nuclear Medicine 2018;59(6):915–21. [PubMed: 29191855]
19. Nockel P, Millo C, Keutgen X, Klubo-Gwiezdzinska J, Shell J, Patel D, et al. The Rate and Clinical Significance of Incidental Thyroid Uptake as Detected by Gallium-68 DOTATATE Positron Emission Tomography/Computed Tomography. Thyroid 2016;26(6):831–5. [PubMed: 27094616]
20. Chang CA, Pattison DA, Tothill RW, Kong G, Akhurst TJ, Hicks RJ, et al. (68)Ga-DOTATATE and (18)F-FDG PET/CT in Paraganglioma and Pheochromocytoma: utility, patterns and heterogeneity. Cancer Imaging 2016;16(1):22. [PubMed: 27535829]
21. Taelman VF, Radojewski P, Marincek N, Ben-Shlomo A, Grotzky A, Olariu CI, et al. Upregulation of Key Molecules for Targeted Imaging and Therapy. Journal of nuclear medicine : official publication, Society of Nuclear Medicine 2016;57(11):1805–10. [PubMed: 27363833]
22. Harvey JM, Clark GM, Osborne CK, and Allred DC. Estrogen receptor status by immunohistochemistry is superior to the ligand-binding assay for predicting response to adjuvant endocrine therapy in breast cancer. J Clin Oncol 1999;17(5):1474–81. [PubMed: 10334533]
23. Zhang L, Gaskins K, Yu Z, Xiong Y, Merino MJ, and Kebebew E. An in vivo mouse model of metastatic human thyroid cancer. Thyroid 2014;24(4):695–704. [PubMed: 24262022]
24. Zhang L, Vines DC, Scollard DA, McKee T, Komal T, Ganguly M, et al. Correlation of Somatostatin Receptor-2 Expression with Gallium-68-DOTA-TATE Uptake in Neuroblastoma Xenograft Models. Contrast Media Mol Imaging 2017;2017:9481276. [PubMed: 29097943]
25. Integrated genomic characterization of papillary thyroid carcinoma. Cell 2014;159(3):676–90. [PubMed: 25417114]
26. Sharma R, Wang WM, Yusuf S, Evans J, Ramaswami R, Wernig F, et al. (68)Ga-DOTATATE PET/CT parameters predict response to peptide receptor radionuclide therapy in neuroendocrine tumours. Radiotherapy and oncology : journal of the European Society for Therapeutic Radiology and Oncology 2019;141:108–15. [PubMed: 31542317]
27. Zhang J, Kulkarni HR, Singh A, Niepsch K, Müller D, and Baum RP. Peptide Receptor Radionuclide Therapy in Grade 3 Neuroendocrine Neoplasms: Safety and Survival Analysis in 69 Patients. Journal of nuclear medicine : official publication, Society of Nuclear Medicine 2019;60(3):377–85. [PubMed: 30115686]
28. Kayani I, Bomanji JB, Groves A, Conway G, Gacinovic S, Win T, et al. Functional imaging of neuroendocrine tumors with combined PET/CT using 68Ga-DOTATATE (DOTA-DPhe1,Tyr3-octreotate) and 18F-FDG. Cancer 2008;112(11):2447–55. [PubMed: 18383518]
29. Mojtahedi A, Thamake S, Tworowska I, Ranganathan D, and Delpassand ES. The value of (68)Ga-DOTATATE PET/CT in diagnosis and management of neuroendocrine tumors compared to current FDA approved imaging modalities: a review of literature. American journal of nuclear medicine and molecular imaging 2014;4(5):426–34. [PubMed: 25143861]
30. Budiawan H, Salavati A, Kulkarni HR, and Baum RP. Peptide receptor radionuclide therapy of treatment-refractory metastatic thyroid cancer using (90)Yttrium and (177)Lutetium labeled somatostatin analogs: toxicity, response and survival analysis. American journal of nuclear medicine and molecular imaging 2013;4(1):39–52. [PubMed: 24380044]

31. Lapa C, Werner RA, Schmid JS, Papp L, Zsótér N, Biko J, et al. Prognostic value of positron emission tomography-assessed tumor heterogeneity in patients with thyroid cancer undergoing treatment with radiopeptide therapy. Nuclear medicine and biology 2015;42(4):349–54. [PubMed: 25595135]
32. Versari A, Sollini M, Frasoldati A, Fraternali A, Filice A, Froio A, et al. Differentiated thyroid cancer: a new perspective with radiolabeled somatostatin analogues for imaging and treatment of patients. Thyroid : official journal of the American Thyroid Association 2014;24(4):715–26. [PubMed: 24102584]
33. Alsadik S, Yusuf S, and Al-Nahhas A. Peptide Receptor Radionuclide Therapy for Pancreatic Neuroendocrine Tumours. Curr Radiopharm 2019;12(2):126–34. [PubMed: 30714538]
34. Roll W, Riemann B, Schafers M, Stegger L, and Vrachimis A. 177Lu-DOTATATE Therapy in Radioiodine-refractory Differentiated Thyroid Cancer: A Single Center Experience. Clin Nucl Med 2018;43(10):e346–e51. [PubMed: 30059430]
35. Veenstra MJ, van Koetsveld PM, Dogan F, Farrell WE, Feelders RA, Lamberts SWJ, et al. Epidrug-induced upregulation of functional somatostatin type 2 receptors in human pancreatic neuroendocrine tumor cells. Oncotarget 2018;9(19):14791–802. [PubMed: 29599907]
36. Torrisani J, Hanoun N, Laurell H, Lopez F, Maoret JJ, Souque A, et al. Identification of an upstream promoter of the human somatostatin receptor, hSSTR2, which is controlled by epigenetic modifications. Endocrinology 2008;149(6):3137–47. [PubMed: 18325993]
37. Guenter RE, Aweda T, Carmona Matos DM, Whitt J, Chang AW, Cheng EY, et al. Pulmonary Carcinoid Surface Receptor Modulation Using Histone Deacetylase Inhibitors. Cancers (Basel) 2019;11(6).
38. Jin XF, Auernhammer CJ, Ilhan H, Lindner S, Nolting S, Maurer J, et al. Combination of 5-Fluorouracil with Epigenetic Modifiers Induces Radiosensitization, Somatostatin Receptor 2 Expression, and Radioligand Binding in Neuroendocrine Tumor Cells In Vitro. Journal of nuclear medicine : official publication, Society of Nuclear Medicine 2019;60(9):1240–6. [PubMed: 30796167]
39. Trinka E, Hofler J, Zerbs A, and Brigo F. Efficacy and safety of intravenous valproate for status epilepticus: a systematic review. CNS Drugs 2014;28(7):623–39. [PubMed: 24806973]
40. Zhu W, Cheng Y, Wang X, Yao S, Jia R, Xu J, et al. Head-to-head comparison of (68)Ga-DOTA-JR11 and (68)Ga-DOTATATE PET/CT in patients with metastatic, well-differentiated neuroendocrine tumors: a prospective study. Journal of nuclear medicine : official publication, Society of Nuclear Medicine 2019.
41. Wild D, Fani M, Fischer R, Del Pozzo L, Kaul F, Krebs S, et al. Comparison of somatostatin receptor agonist and antagonist for peptide receptor radionuclide therapy: a pilot study. Journal of nuclear medicine : official publication, Society of Nuclear Medicine 2014;55(8):1248–52. [PubMed: 24963127]
42. Liu Q, Cheng Y, Zang J, Sui H, Wang H, Jacobson O, et al. Dose escalation of an Evans blue-modified radiolabeled somatostatin analog (177)Lu-DOTA-EB-TATE in the treatment of metastatic neuroendocrine tumors. Eur J Nucl Med Mol Imaging 2019.
43. Wang H, Cheng Y, Zhang J, Zang J, Li H, Liu Q, et al. Response to Single Low-dose (177)Lu-DOTA-EB-TATE Treatment in Patients with Advanced Neuroendocrine Neoplasm: A Prospective Pilot Study. Theranostics 2018;8(12):3308–16. [PubMed: 29930731]

Translational relevance statement:

We demonstrated that somatostatin receptor type 2 (SSTR2) may serve as a molecular target in the diagnosis and treatment of a subset of thyroid cancer (TC) patients. We showed that TC lesions have higher SSTR2 expression than normal thyroid. Further, we reported high uptake of SST analog ^{68}Ga-DOTA-TATE in a subset of TC patients, particularly in Hurthle-cell TC resistant to standard treatment. *In vivo* studies demonstrated that the theranostic efficacy of SST analogs could be enhanced by utilizing radiolabeled DOTA-EB-TATE, which is characterized by significantly higher tumor uptake than DOTA-TATE and DOTA-JR11. Treatment with ^{177}Lu-DOTA-EB-TATE extended survival and reduced tumor size in a mouse model with high-SST analog uptake, comparable with the uptake observed in human Hurthle-cell TC. Overall, ^{177}Lu-DOTA-EB-TATE has the potential to be translated from bench to bedside for the targeted therapy of TC patients characterized by high tumor uptake of SST analogs.

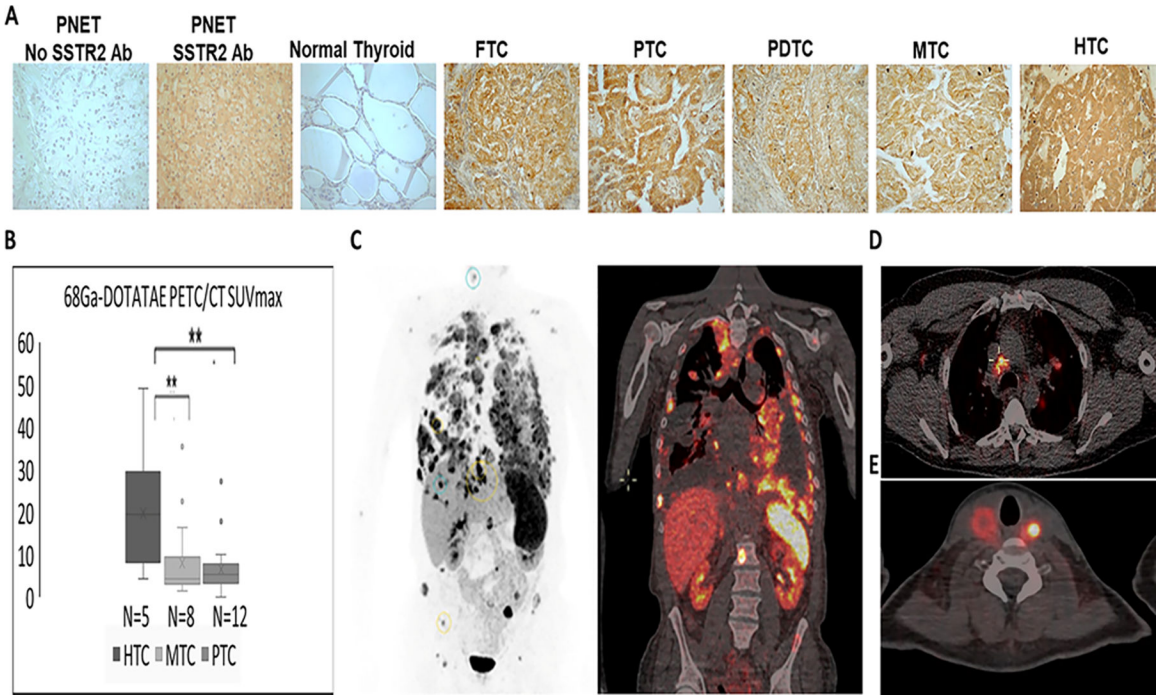

Figure 1. A subset of thyroid cancer patients is characterized by moderate to high ^{68}Ga-DOTA-TATE uptake.

(A) Representative images showing increased expression of SSTR2 in TC compared with normal thyroid documented by immunostaining (Supplemental Table 1). PNET – positive control-pancreatic neuroendocrine tumor; No SSTR2 Antibodies (Ab) – negative control; FTC- follicular thyroid cancer, PTC- papillary thyroid cancer, PDTC – poorly differentiated thyroid cancer, MTC – medullary thyroid cancer, HTC – Hürthle cell thyroid cancer

(B) Significantly higher ^{68}Ga-DOTA-TATE uptake in patients with Hürthle cell thyroid cancer (HTC) (14 metastatic lesions analyzed in 5 patients), compared with medullary thyroid cancer (MTC) (24 metastatic lesions analyzed in 8 patients), and papillary thyroid cancer (PTC) (36 metastatic lesions analyzed in 12 patients).

(C) ^{68}Ga-DOTA-TATE PET (black and white) and PET/CT (soft tissue window) imaging in a patient with metastatic HTC (SUV_{max} ranging between 16.5–33).

(D) ^{68}Ga-DOTA-TATE PET/CT imaging in a patient with metastatic PTC (SUV_{max} ranging between 17.9–27.2).

(E) ^{68}Ga-DOTA-TATE PET/CT imaging in a patient with metastatic MTC with an intact thyroid (thyroid tumor uptake SUV_{max} ranging between 9.4–35.5).

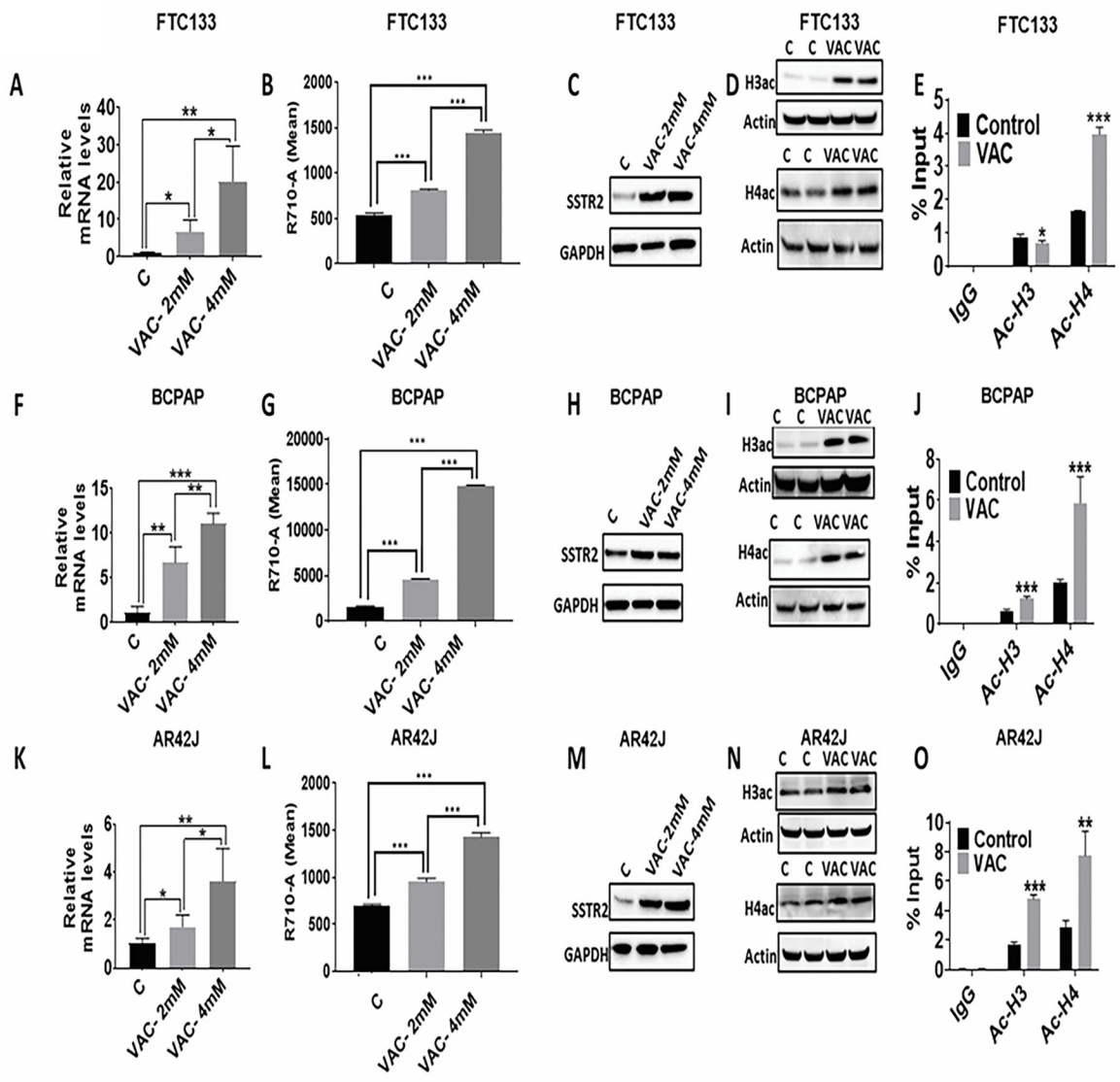

Figure 2: Valproic acid -associated increased histone acetylation is associated with higher SSTR2 expression in thyroid cancer cells.

(A, F, K) An increase in SSTR2 mRNA expression in FTC133 (n=4), BCPAP (n=4), and AR42J cells (n=4) upon VAC treatment (2mM and 4Mm; 72h). ***p<0.001, **p<0.01, *p<0.05. C-control; VAC-valproic acid.

(B, G, L) An increase in surface expression of SSTR2 expression in FTC133 (n=3), BCPAP (n=3), and AR42J cells (n=3) upon VAC treatment (2mM and 4Mm; 72h). ***p<0.001. C-control; VAC-valproic acid.

(C, H, M) An increase in SSTR2 protein expression in FTC133 (n=3), BCPAP (n=3), and AR42J cells (n=3) upon VAC treatment (2mM and 4mM; 72h). C-control; VAC-valproic acid.

(D, I, N) An increase in global histone acetylation (H3ac and H4ac) at the protein level in FTC133 (n=3), BCPAP (n=3), and AR42J cells (n=3) upon VAC treatment (4mM; 72h). C-control; VAC-valproic acid.

(E, J, O) An increase in the amount of H4ac at the SSTR2 promoter in FTC133 (n=4), BCPAP (n=4), and AR42J cells (n=4) upon VAC treatment (4mM; 72h). An increase in the amount of H3ac at the SSTR2 promoter observed in BCPAP (n=4) and AR42J cells (n=4) upon VAC treatment (4mM). ***p<0.001, **p<0.01, *p<0.05 w.r.t Control. C-control; VAC-valproic acid.

Data are presented as mean±SD.

The SSTR2 antibodies used in the study had a lower affinity for rat than human SSTR2 epitope leading to weak signals despite very high SST analog uptake in AR42J cells.

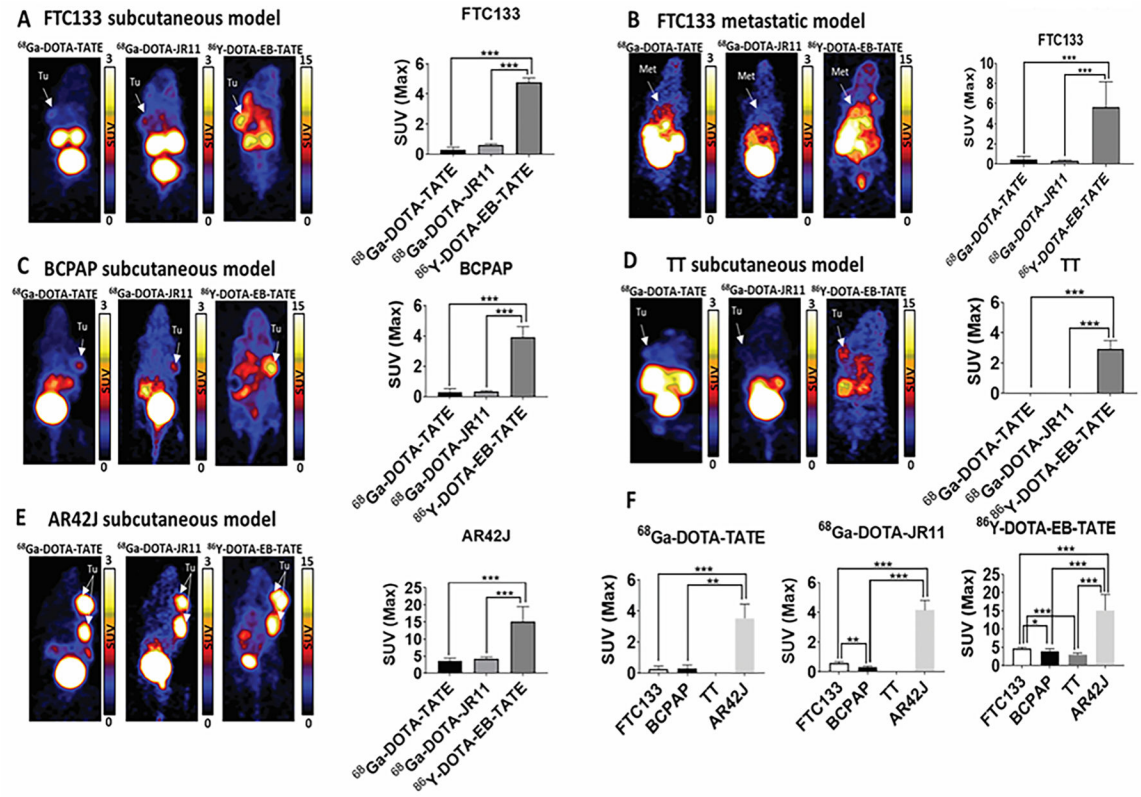

Figure 3: DOTA-EB-TATE is a superior SST analog in comparison to DOTA-TATE and DOTA-JR11. High-SSTR2-expressing AR42J tumors are characterized by superior uptake of SST analogs compared to low-SSTR2-expressing FTC133, BCPAP, and TT tumors.

(A) Representative PET images comparing uptake of ^{68}Ga-DOTA-TATE, ^{68}Ga-DOTA-JR11, ^{86}Y-DOTA-EB-TATE in FTC133 subcutaneous xenograft mice model. The bar graph shows a significantly higher uptake of ^{86}Y-DOTA-EB-TATE in comparison to ^{68}Ga-DOTA-TATE and ^{68}Ga-DOTA-JR11 in FTC133 (n=5) subcutaneous mice model. ***p<0.001.

(B) Representative PET images comparing uptake of ^{68}Ga-DOTA-TATE, ^{68}Ga-DOTA-JR11, ^{86}Y-DOTA-EB-TATE in FTC133 metastatic mice model. The bar graph shows a significantly higher uptake of ^{86}Y-DOTA-EB-TATE in comparison to ^{68}Ga-DOTA-TATE and ^{68}Ga-DOTA-JR11 in FTC133 (n=8–12) metastatic mice model. ***p<0.001.

(C) Representative PET images comparing the uptake of ^{68}Ga-DOTA-TATE, ^{68}Ga-DOTA-JR11, ^{86}Y-DOTA-EB-TATE in BCPAP subcutaneous xenograft mice model. The bar graph shows a significantly higher uptake of ^{86}Y-DOTA-EB-TATE in comparison to ^{68}Ga-DOTA-TATE and ^{68}Ga-DOTA-JR11 in BCPAP (n=3) subcutaneous mice model. ***p<0.001.

(D) Representative PET images comparing uptake of ^{68}Ga-DOTA-TATE, ^{68}Ga-DOTA-JR11, ^{86}Y-DOTA-EB-TATE in TT subcutaneous xenograft mice model. The bar graph shows a significantly higher uptake of 86Y-DOTA-EB-TATE in comparison to ^{68}Ga-DOTA-TATE and ^{68}Ga-DOTA-JR11 in TT (n=5) subcutaneous mice model. ***p<0.001.

(E) Representative PET images comparing uptake of ^{68}Ga-DOTA-TATE, ^{68}Ga-DOTA-JR11, ^{86}Y-DOTA-EB-TATE in AR42J subcutaneous xenograft mice model. The bar graph shows a significantly higher uptake of ^{86}Y-DOTA-EB-TATE in comparison to ^{68}Ga-DOTA-TATE and ^{68}Ga-DOTA-JR11 in AR42J (n=4) subcutaneous mice model. ***p<0.001.

(F) The bar graph compares FTC133 (n=5), BCPAP (n=3), TT (n=5), and AR42J (n=4) subcutaneous mice models for the uptake of ^{68}Ga-DOTA-TATE, ^{68}Ga-DOTA-JR11 and ^{86}Y-DOTA-EB-TATE. ^{86}Y-DOTA-EB-TATE has the highest uptake in comparison to ^{68}Ga-DOTA-TATE and ^{68}Ga-DOTA-JR11 in all the mice models. *$p<0.05$, **$p<0.01$, ***$p<0.001$.

Tumors (Tu) and metastasis (Met) are indicated by white arrows. The SUV scales range from 0 to 3 for ^{68}Ga-DOTA-TATE and ^{68}Ga-DOTA-JR11 and 0 to 15 for ^{86}Y-DOTA-EB-TATE. Data are presented as mean±SD.

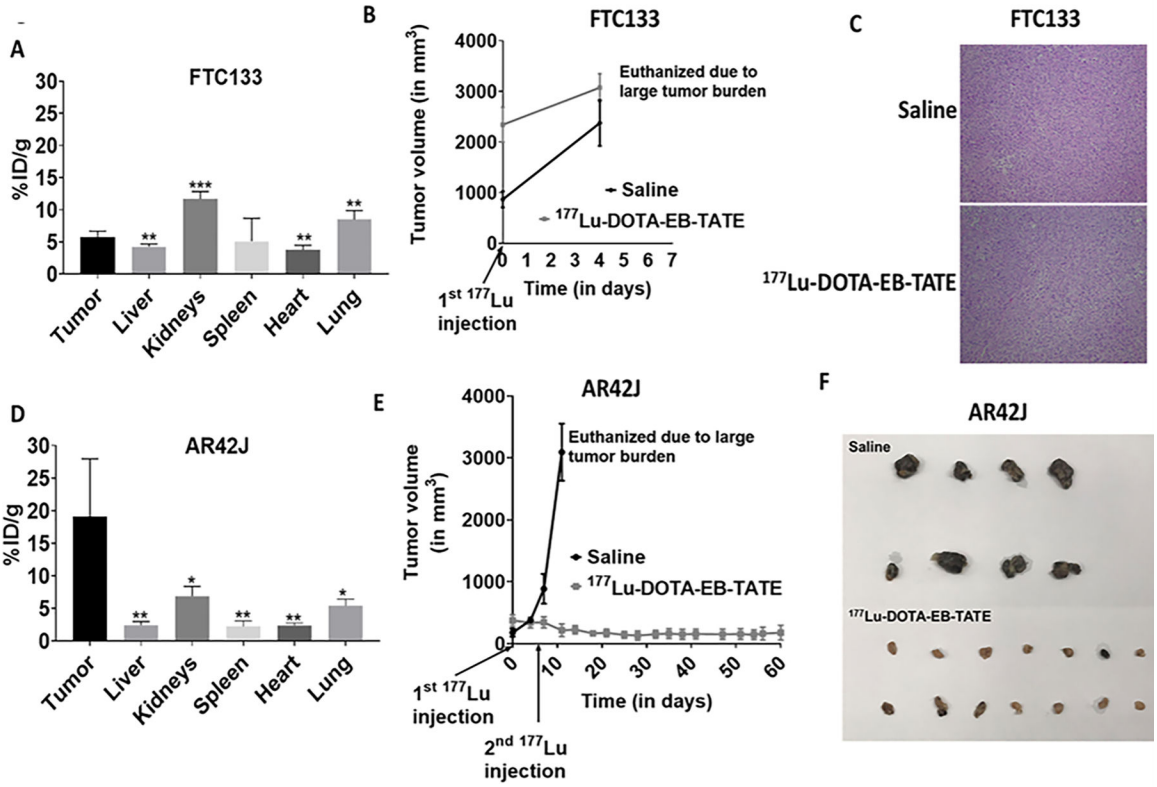

Figure 4: Treatment with DOTA-EB-TATE promotes tumor regression and progression-free survival in high-SSTR2-expressing tumors.

(A) The bar graph shows quantification of ^{86}Y-DOTA-EB-TATE in the tumor and normal tissues (liver, kidneys, spleen, heart, and lungs) of the FTC133 subcutaneous xenograft mice (n=5). ***p<0.001, **p<0.01 w.r.t tumor tissue.

(B) No effect of PRRT on FTC133 (low-SSTR2-expressing) subcutaneous xenograft mice receiving ^{177}Lu-DOTA-EB-TATE treatment (n=8) in comparison to the mice that received saline (n=4). Data are presented as mean±SEM.

(C) Representative hematoxylin-eosine (H-E) stained slides show no difference in the histology of FTC133 tumors derived from the saline and ^{177}Lu-DOTA-EB-TATE treated mice.

(D) The bar graph shows quantification of ^{86}Y-DOTA-EB-TATE in the tumor and normal tissues (liver, kidneys, spleen, heart, and lungs) of the AR42J subcutaneous xenograft mice (n=4). **p<0.01, *p<0.05 w.r.t tumor tissue.

(E) Significant reduction in the tumor volume of the AR42J (high-SSTR2-expressing) subcutaneous xenograft mice that received ^{177}Lu-DOTA-EB-TATE treatment (n=8) in comparison to the saline treated mice (n=4). Data are presented as mean±SEM.

(F) Representative images of the tumor tissues collected after euthanasia from saline and ^{177}Lu-DOTA-EB-TATE treated AR42J subcutaneous xenograft mice.

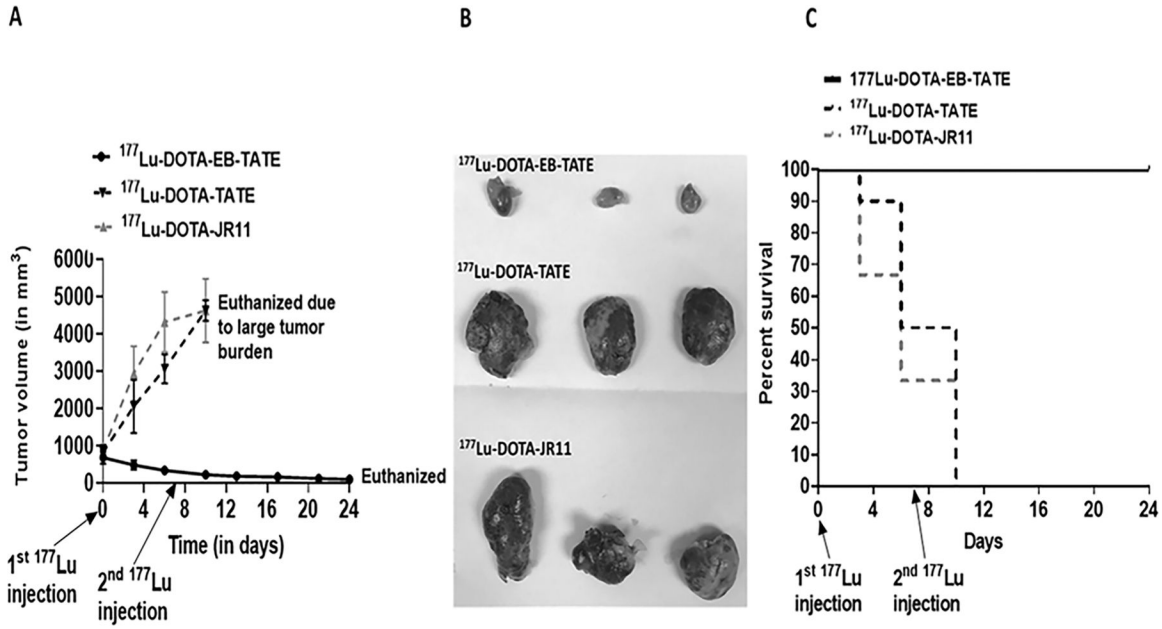

Figure 5: DOTA-EB-TATE is a superior SST analog in the treatment of SSTR2 expressing tumors.

(A) Significant reduction in the tumor volume of the AR42J subcutaneous mice model on treatment with ^{177}Lu-DOTA-EB-TATE (n=9) in comparison to the ^{177}Lu-DOTA-TATE (n=10) and ^{177}Lu-DOTA-JR11 (n=9). Data are presented as mean±SEM.

(B) Representative images of the tumor tissues collected after euthanasia from ^{177}Lu-DOTA-EB-TATE, ^{177}Lu-DOTA-TATE, ^{177}Lu-DOTA-JR11 treated AR42J subcutaneous xenograft mice.

(C) Kaplan-Meier survival curve comparing disease-specific survival (DSS) among different SST analogs in AR42J subcutaneous xenograft mice. The graph depicts significantly longer DSS of the ^{177}Lu-DOTA-EB-TATE treated mice in comparison to ^{177}Lu-DOTA-TATE and ^{177}Lu-DOTA-JR11 treated mice.

Table 1.

Comparison of the maximum standard uptake values (SUV_{max}) of radiolabeled SST analogs in FTC133, BCPAP, TT, and AR42J subcutaneous xenograft mice models.

Cell lines	Uptake of radiolabeled SST analogs (SUV_{max} ± S.D)			p-value		
	^{68}Ga-DOTA-TATE	^{68}Ga-DOTA-JR11	^{86}Y-DOTA-EB-TATE	^{68}Ga-DOTA-TATE vs ^{68}Ga-DOTA-JR11	^{68}Ga-DOTA-TATE vs ^{68}Ga-DOTA-EB-TATE	^{68}Ga-DOTA-JR11 vs ^{68}Ga-DOTA-EB-TATE
FTC133	0.28±0.19	0.59±0.1	4.8±0.27	0.0668	<0.0001	<0.0001
BCPAP	0.28±0.25	0.34±0.06	3.92±0.7	0.985	0.0001	0.0001
TT	0±0	0±0	2.94±0.55	>0.9999	<0.0001	<0.0001
AR42J	3.53±0.91	4.14±0.65	15.16±4.34	0.9407	0.0003	0.0005